Stacking-Dependent Interlayer Magnetic Coupling 2D $CrI_3/CrGeTe_3$ Nanostructures for Spintronics

Jing Shang[1], Xiao Tang[1], Xin Tan[2], Aijun Du[1], Ting Liao[1], Sean C. Smith[2], Yuantong Gu[1], Chun Li[3], Liangzhi Kou[1*]

[1]*School of Chemistry, Physics and Mechanical Engineering Faculty, Queensland University of Technology, Gardens Point Campus, QLD 4001, Brisbane, Australia*

[2]*Department of Applied Mathematics, Research School of Physics and Engineering, Australian National University, Canberra 2601, Australia*

[3]*School of Mechanics, Civil Engineering and Architecture, Northwestern Polytechnical University, Xi'an 710072, China*

Corresponding Author

*E-mail: liangzhi.kou@qut.edu.au

School of Chemistry, Physics and Mechanical Engineering Faculty, Queensland University of Technology, Gardens Point Campus, QLD 4001, Brisbane, Australia

ABSTRACT. The recent emergence of two-dimensional (2D) materials with intrinsic long-range magnetic order opens the avenue of fundamental physics studies and the spintronic application, however, the mechanism of interlayer magnetic coupling and the feasible way to control magnetic states are yet to be fully investigated. In the present study, from first principle calculations, we studied the interlayer magnetic coupling of 2D CrI_3/$CrGeTe_3$ heterostructures and revealed the stacking dependent magnetic states, it is found that AB and AB_1 stacking prefers to the ferromagnetic interlayer coupling while other two stacked configurations are in ferrimagnetic state. The underlying mechanism is contributed to the competition between nearest neighbour (NN) and second nearest neighbour (SNN) Cr-Cr atoms between layers. Meanwhile, it is also found the electronic properties are stacking dependent while the band edge states are separated to the different layers. The magnetic and electronic states can be effectively tuned by the external strain. Based on the findings, the magnetic domain devices are proposed in the twisted magnetic heterostructures with the domain size and interlayer coupling being controlled by the rotation angle. Our study thus provides an approach to achieve the controllable magnetic/electronic properties which is not only important for the fundamental researches, but also useful for the practically applications in spintronics.

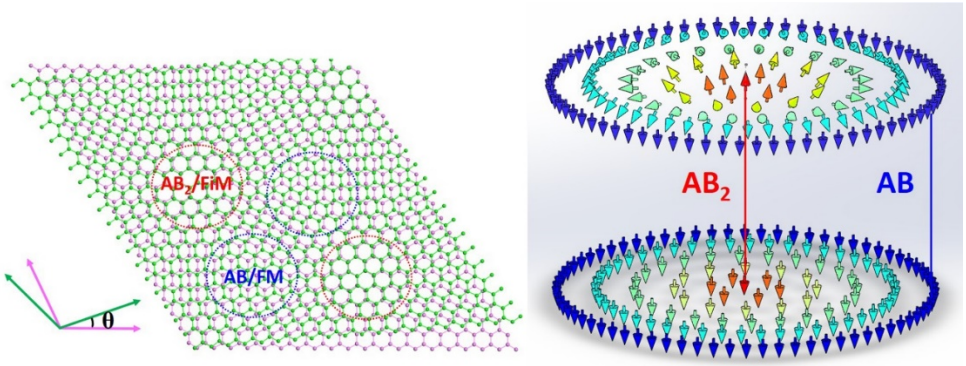

1. Introduction

In recent years, two-dimensional (2D) materials[1] have attracted great attention due to the unique electronic/mechanical properties[2-5] and the novel electronics and energy conversion applications. 2D magnet, as a special family, is particularly promising for novel functional spintronic devices with low energy cost and high storage density.[6-8] Although the existence of the long-range ferromagnetic (FM) order in 2D size was doubted due to the thermal fluctuation in low-dimensional scale according to the Mermin-Wagner theorem,[9] the issue is expected to be solved as indicated by recent studies. The magnetic anisotropy will help to stabilize the long-range FM order at finite temperatures and lift the Mermin-Wagner restriction, therefore starting the research era of 2D magnetic materials. As the examples, the layered $Cr_2Ge_2Te_6$ [10] and monolayer CrI_3 [11] have been experimentally synthesized and confirmed to be intrinsic 2D anisotropy FM materials. The FM order can be persisted within each layer due to the superexchange coupling in perpendicular Cr-I-Cr in monolayer CrI_3 [12], but the interlayer magnetic coupling is usually dominated as antiferromagnetic (AFM) or ferromagnetic (FM) orders depending on the layer number and coupling[12]. Moreover, since the tunable magnetic couplings between 2D magnets layers depend sensitively on the interlayer correlation [13], it has been discovered that the magnetic couplings between CrI_3 layers could be switched by various external fields such as electric field [14], electron doping [15-17] or strain [18], rendering the monolayer magnets favorable candidates for the application in spintronic devices. Those findings revealed the importance of interlayer coupling for magnetic system, but the systematic understanding is absent.

With distinct electronic properties, the van der Waals 2D heterostructures which combine different layers together will lead to novel physics and multi-functionality, rendering more enormous variability in terms of tuning and controlling properties. For example, the localization of Dirac electrons and a new set of Dirac fermions were discovered in rotated graphene bilayers [19] and graphene/BN heterostructures[20], respectively. Meanwhile, the spin-orbit interaction of graphene layer in graphene/WS_2[21] can be enhanced, leading to strong quantum spin hall effect, the photoexcited electrons and holes in MoS_2/WSe_2 heterojunctions [22] would be accumulated at the interface, which can find extensive application in photovoltaic applications. Taking advantage of the intrinsic magnetism of CrI_3 monolayer, more fascinating phenomenon have been revealed such as the strong magnetization from graphene of CrI_3/graphene heterostructure [23] and the valley manipulation of WSe_2 by magnetic CrI_3 layer

in CrI_3/WSe_2 heterojunction [24].. Although substantial research endeavors have been devoted to the utilization of magnetism of 2D magnets in various heterojunction systems, the magnetic behaviors in layered heterostructures which combine two magnetic layers together like $CrI_3/Cr_2Ge_2Te_6$ remains unexplored to date. Based on the successful exfoliation of CrI_3 and $CrGeTe_3$ monolayers from bulk crystals, the magnetic heterostructure is expected to be fabricated with physical transfer and stacking method.

Therefore, in the present study, the magnetic heterostructure based on 2D magnets (CrI_3 and $Cr_2Ge_2Te_6$) is proposed by the density functional theory (DFT) calculations, which is relatively facilely fabricated due to their similar lattice parameter. The magnetic behaviors of $CrI_3/Cr_2Ge_2Te_6$ heterostructures tuned and controlled by stacking orders and external fields are also discussed. The tunability of magnetic and electronic properties in stacking-dependent suggests potential new approaches to engineer the magnetic materials structures for possible future applications.

2. Computational Methods.

The present calculations have been performed by using the VASP simulation package [25] with spin-polarization and the projector augmented-wave (PAW) method [26] to describe the ion-electron interaction and electron spin effect. General gradient approximation (GGA) in the Perdew-Burke-Ernzerhof (PBE) implementation [27] is applied as the exchange correlation functional. As the effective onsite coulomb interaction of 3*d* electrons of the transition metals play a significant role in electronic properties, in order to take into account the effect of the strong localization of the Cr *d* electron, we also performed PBE+U calculations. The same as the previous investigations, the Hubbard U value is set to be 3.0 eV, which can well re-produce the magnetic state. Zero damping DFT-D3 with the Grimme vdW correction [28] (where D stands for dispersion) method was adopted to account for the interlayer van der Waals forces between CrX_3 and $CrGeTe_3$ layers. A large vacuum space of at least 30 Å thick is included along the direction that is perpendicular to *ab* plane to avoid interaction between images. The atomic positions were fully relaxed until the energy and force differences are converged within 10^{-5} eV and 10^{-3} eV/Å, respectively, to minimize the quantum mechanical stresses and forces. The energy cutoff was adopted as 400 eV throughout the entire calculations. The Brillouin zone was represented by Monkhost-Pack special k-point mesh [29] of 11×11×1. The band structures of $CrI_3/CrGeTe_3$ heterostructures is calculated along the special lines of M (0.0, 0.5, 0.0) → G

(0.0, 0.0, 0.0) → K (-1/3, 1/3, 0.0) → M (0.0, 0.5, 0.0). Gaussian smearing with a smearing width of 0.1 meV is used in the Brillouin zone integration.

For strain-modified CrI_3/$CrGeTe_3$ heterostructures system, biaxial strains were applied along *xy*-plane by elongating the lattice constants of the equilibrium structure a_0 to a ($a= a_0+\Delta a$) and b_0 to b ($b= b_0+\Delta b$). The strain was defined as $\varepsilon= \Delta a/a_0$, same as the ratio of $\Delta b/b_0$.

3. Results and Discussions

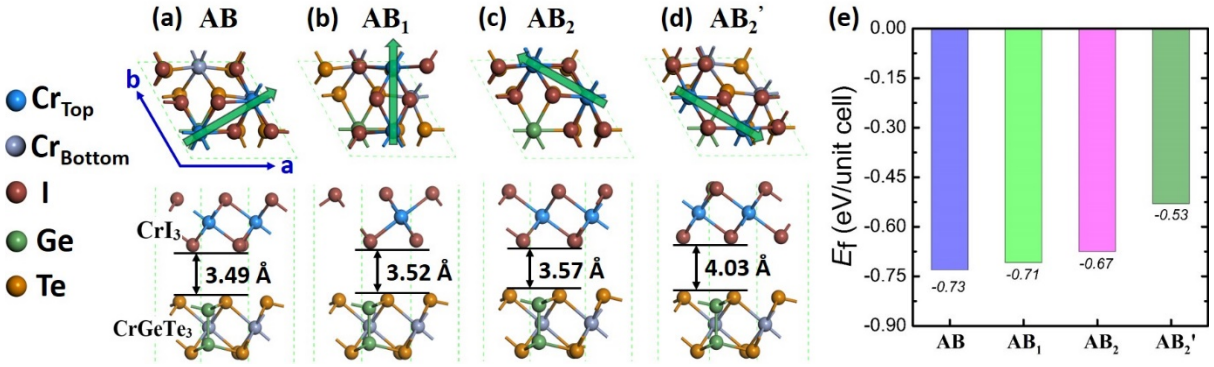

Figure 1. Crystal structures for different stacked CrI_3/$CrGeTe_3$ heterostructures. (a-d) Top and side view of the heterostructure under different stacking patterns. For clarity, the Cr atoms in CrI_3 and $CrGeTe_3$ layers are shown by different colours. Blue (grey) balls represent the Cr atoms in the CrI_3 ($CrGeTe_3$) layer. The green arrows have marked the different position arrangements of Cr positions in CrI_3 with $CrGeTe_3$ unchanged. (e) The formation energies of the heterostructures.

As the interlayer space is largely determined by stacking patterns, which will affect the strength of magnetic coupling, we therefore begin our discussion with the stacking configurations of CrI_3/$CrGeTe_3$ heterostructures. The lattice parameters of CrI_3 and $CrGeTe_3$ are very close to each other (6.905 and 6.913 Å, respectively), the heterostructures can thus be constructed simply using the primitive cells of CrI_3 and $CrGeTe_3$ with negligible lattice mismatch. The hexagonal crystal structures with four different stacking orders are adopted corresponding to the relatively different geometries, as shown in Figure 1 a-d. Magnetic Cr ions of monolayer $CrGeTe_3$ forms a honeycomb lattice, which is labelled as "A"-block and kept unchanged for all the studied models. Then monolayer CrI_3 labelled as "B"-block is stacked on top of $CrGeTe_3$ layer. Depending on the relative position of Cr atoms, the heterostructures can be classified into four different stacking orders, namely AB, AB_1, AB_2 and AB_2' as shown in Figure 1. For AB stacking, in the unit cell one of Cr atoms of CrI_3 is on top of the Cr from $CrGeTe_3$ while another is located at the hexagonal centre of bottom layer. With respect to the AB-stacking, the AB_1 and AB_2 configurations can be obtained by rotating the CrI_3 layer of 60° and 120° relative

to bottom layer $CrGeTe_3$ marked as green arrows in Figure 1 a-c. For AB_2 stacking, both Cr atoms from CrI_3 unit-cell are on top of corresponding Cr atoms of $CrGeTe_3$. For AB_2' stacking, the CrI_3 layer is rotated by 300° relative to the CrI_3 layer in AB stacking since the structures with rotations of 180° and 240° would produce the same stacking orders as AB, AB_1 due to the mirror symmetric $CrGeTe_3$ layer. After the fully structural relaxations, the lattice constant of the heterostructures is optimized as a = b = 6.91 Å. While the interlayer distances are strongly stacking dependent, which are 3.45, 3.52, 3.57 and 4.03 Å for four stacking patterns respectively, implying the different interlayer vdW strengths and magnetic coupling. To estimate the structural stabilities of the heterostructures under different stacking patterns, we calculated the formation energies, which are defined as E_f=E_{tot}-E_{CrI3}-$E_{CrGeTe3}$, here E_{tot} is the total energy of the heterostructure, E_{CrI3} ($E_{CrGeTe3}$) is the energy of isolated CrI_3 ($CrGeTe_3$) layer. The results shown in Figure 1e indicate that AB stacked heterostructure is the most stable with the formation energy of -0.73 eV/unitcell, AB_1 stacking is the second most stable one with -0.71 eV/unitcell. The AB_2 and AB_2' structures are obviously less stable; the formation energies are -0.67 and -0.53 eV/unicell respectively. It's worthy to point out that the interlayer distances and the formation energies were calculated based on the magnetic ground state for each stacking order, namely FM for AB and AB_1, ferrimagnetic (FiM) for AB_2 and AB_2' stacking which will be discussed in detailed in the following part. Regardless of the stacking patterns, all the heterostructures have the negative formation energies, indicating that they are energetically favourable and should be experimentally achievable. Based on the fact that both 2D CrI_3 and $CrGeTe_3$ monolayers have been experimentally synthesized and all stacking patterns are energetically preferred, it is feasible to fabricate the magnetic heterostructure in the near future.

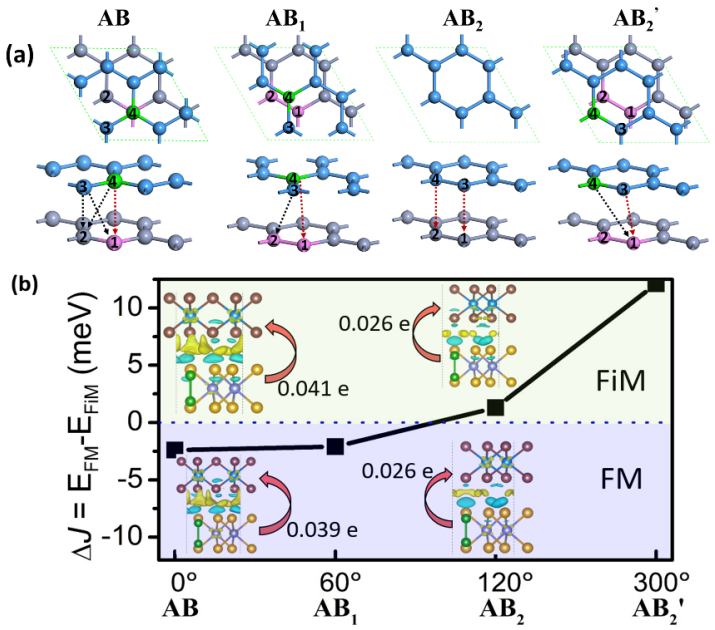

Figure 2. (a) The stacking configurations of Cr atoms extracted from the CrI_3/$CrGeTe_3$ heterostructures with various stacking orders. All atoms except Cr are not shown for clarity. The red and black arrows show the nearest neighbour and the second nearest neighbour Cr-Cr configurations of CrI_3 and $CrGeTe_3$ layers, respectively. The green and pink atoms are marked to distinguish the positions of Cr atoms in each layer. The blue and gray balls present Cr in CrI_3 and $CrGeTe_3$ layers, respectively. (b) The energy difference (ΔJ) between FM and FiM. The insets in (b) present the differential charge density for AB and AB_2 stacking orders with FM and FiM spin configurations. The isosurface value is set to 0.0002 e/Å^3.

To figure out the magnetic ground state of the heterostructures, the corresponding total energies for FM and ferrimagnetic (FiM: Cr atoms from different layers have opposite spin direction, but the corresponding magnitude of magnetic moments are different, leading to non-zero total magnetic moment) states have been examined by energetic calculations. The interlayer exchange energy $\Delta J = E_{FM} - E_{FiM}$ were then calculated to determine the magnetic preferred state. The negative value indicates the lower energy of FM state. Since the intralayer magnetic coupling of CrI_3 ($CrGeTe_3$) is FM with the nearest two Cr atoms aligning parallel due to the Cr-I-Cr (Cr-Te-Cr) superexchange coupling,[30] we arrange all the Cr atom in one layer with the same spin direction. The results as summarized at Figure 2 show that the magnetic ground state strongly depend on the stacking orders, AB- and AB_1- stacking configurations prefer FM with the lower total energy by 3 meV/unit, while AB_2 and AB_2' stacking prefer FiM. Especially for AB_2'-stacking structures, the FiM magnetic configuration is 12 meV/unit lower than FM state, indicating strong preference of opposite interlayer spin arrangement. As a result, the total magnetic moments for AB and AB_1 are 12.4 μB (3.1 μB/Cr atom) while the values for AB_2 and AB_2' are -0.2 μB (-0.05 μB). Here it is noticed that even opposite interlayer spin coupling

is found for AB_2 and AB_2' stacked configurations, they still possess the total magnetic moments due to the different spin electron distribution in Cr atom from different layers (3.47 μB/Cr atom of CrI_3; -3.62 μB/Cr atom of $CrGeTe_3$). The interlayer magnetic coupling should directly relate with the electron transfer. As shown by the insets of Figure 2b with AB and AB_2 stacking as typical examples, the electron transfer is also stacking dependent. For AB stacking, about 0.04 e is transferred from $CrGeTe_3$ to CrI_3, but only 0.026 e is transferred for AB_2 stacking. Even for the same stacking, the transfer is also affected by the magnetic coupling as evidenced by AB configuration (0.041e for FiM *vs* 0.039e for FM). For AB_2-stacking, although the total interlayer charge transfer of FM and FiM orders is the same, the amount on the intermediate I and Te atoms are different. Similar conclusions can be also obtained for AB_1 and AB_2' stacking orders [see Figure S1 in Supporting Information].

The stacking dependent magnetic states can be understood from the interlayer magnetic exchange (directly and indirectly) of Cr atoms from different layers. As indicated by previous studies, the intralayer magnetism of CrI_3 or $CrGeTe_3$ was determined as FM by the superexchange of Cr-I-Cr [18] or Cr-Te-Cr [31] when the bond angles are near to 90°, which makes the intralyer FM coupling rather robust. In contrast, AFM coupling is driven by Cr-Cr direct exchange, as explained in previous researches of chromium trihalides and $CrXTe_3$ (X = Si, Ge) [32-34]. In terms of the magnetic coupling between layers, the AFM interaction (FiM in our case here) was ascribed to the interlayer nearest neighbour (NN) exchange of Cr-Cr pairings, while the FM coupling is mainly contributed to the second nearest neighbour (SNN) Cr-Cr interaction which is mediated by I or Te atoms [15, 35]. The stacking-dependent magnetic ground state in the heterostructure will be determined by a competition between NN and SNN interlayer Cr-Cr magnetic couplings. In this sense, we consider the NN and SNN exchanges in $CrI_3/CrGeTe_3$ heterojunctions as well as the affection of the intermediate atoms in our models to reveal the mechanism of magnetic stability. Figure 2a show the relative positions of Cr atoms from different layers for each stacking.

For AB-stacking, there are three SNN (Cr2-Cr3, Cr1-Cr3 and Cr2-Cr4) per unit cell but only one NN corresponding to Cr1-Cr4 pair shown in first panel of Figure 2. Hence, the SNN interaction exchange dominates the magnetic coupling between layers, rendering AB-stacked $CrI_3/CrGeTe_3$ heterojunction prefer FM magnetic state with the total energy of 3 meV/unit lower. For AB_1-stacking, which is the same as AB configuration, it still has 3 SNN and 1 NN Cr-Cr pairs. However due to the relative position shift, the distances of NN and SNN Cr-Cr

interactions are increased compared with these of AB stacking, resulting in weaker interactions of the interlayer magnetic coupling. Therefore, the FM magnetic ground state is still preserved in AB_1 stacking, but the stability is reduced as shown in Figure 2b. As for AB_2-stacking, the strong interlayer FiM coupling originates from dominated NN coupling of the system (all Cr atom of upper layer are on top of these of bottom layer), which makes the competition between NN and SNN negligible in AB_2 configuration. For AB_2'-stacking, it is similar to AB_1 stacking, the combined effect of mediation from I and Te atoms is also applicable, however it possesses 2 SNN and 2 NN Cr-Cr pairs while the interlayer distance is much larger. In terms of magnetism between layers, the competition between NN and SNN super-exchange determines the final magnetic state, AB_2'-stacking prefers FiM alignment derived from the Cr-Cr NN interaction.

Stacking pattern not only affects the interlayer magnetic coupling, but also leads to the stacking dependent electronic properties of $CrI_3/CrGeTe_3$ heterostructures. Here, we still take AB and AB_2 stacking as typical examples with the same reason when discussed the charge transfer above (the corresponding electronic analysis for other two stacking are in supporting information, see Figure S2). Figure 3 shows the band structures and the corresponding density of states (DOS) for $CrI_3/CrGeTe_3$ heterostructures of AB-stacking with FM state and AB_2-stacking with FiM state. Both CrI_3 and $CrGeTe_3$ are the magnetic semiconductors as revealed by previous experimental and theoretical studies. From the electronic calculations, the semiconducting features are well preserved in the magnetic heterostructures, however the band gaps are significantly reduced and stacking dependent. The contributions of electronic states from CrI_3 and $CrGeTe_3$ layers are quite different in the heterostructures. For AB stacked system, it has an indirect band gap of 0.136 eV. In contrast, the band gap of AB_2 stacked heterostructures is only 0.0348 eV. Due to out-of-plane intrinsic polarization which originates from the different electrostatic potential of CrI_3 and $CrGeTe_3$, the band states from CrI_3 will be lifted upward while these from $CrGeTe_3$ are shifted downwards, leading to the staggered band alignments near the Fermi level. Therefore, the band-edge states are contributed from the different layer, where the Conduction band minimum (CBM) is from CrI_3 layer, while the Valence band maximum (VBM) is $CrGeTe_3$ as indicated by the analysis of bandstructure, DOS and wavefunction distribution in Figure 3. The unique electronic properties in the heterostructures will facilitate its application in photovoltaics.

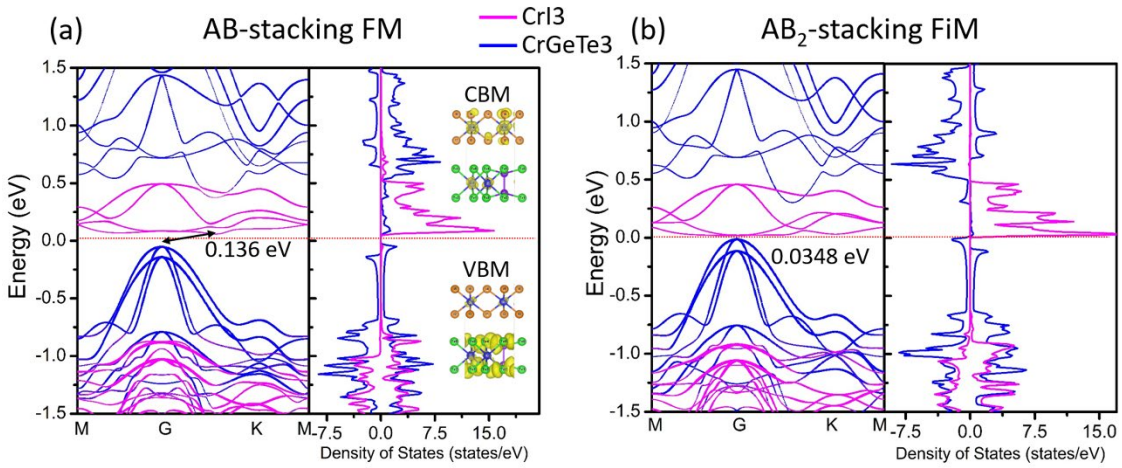

Figure 3. Band structures and density of states (DOS) for CrI_3/$CrGeTe_3$ heterostructures of AB-stacking with FM spin (a) and AB_2-stacking with FiM (b) configuration. The pink and blue lines present the contributions from CrI_3 and $CrGeTe_3$, respectively.

Very recently, the external strategies have been verified to be useful to tune the magnetic states [14]. Song et al. [36] and Li et al. [37] have experimentally realized the controlled interlayer magnetism and the switched magnetic states in layered CrI_3 by external pressure. In our study, as investigated above, the interlayer magnetic coupling of the heterostructures is stacking dependent and determined by the competition of SNN and NN Cr-Cr interaction, it is expected that external strain can modulate the magnetic state since strengths of NN and SNN are sensitive to the Cr-Cr distance. We therefore additionally examined the responses under external biaxial strain which can act as an effective way to control magnetic coupling. The calculated interlayer magnetic exchange energies (ΔJ) as a function of strain are plotted in Figure 4, here we still choose AB and AB_2 stacking patterns for the same reasons as discussed above, the results for other two stacking configurations can be found in the supporting information.

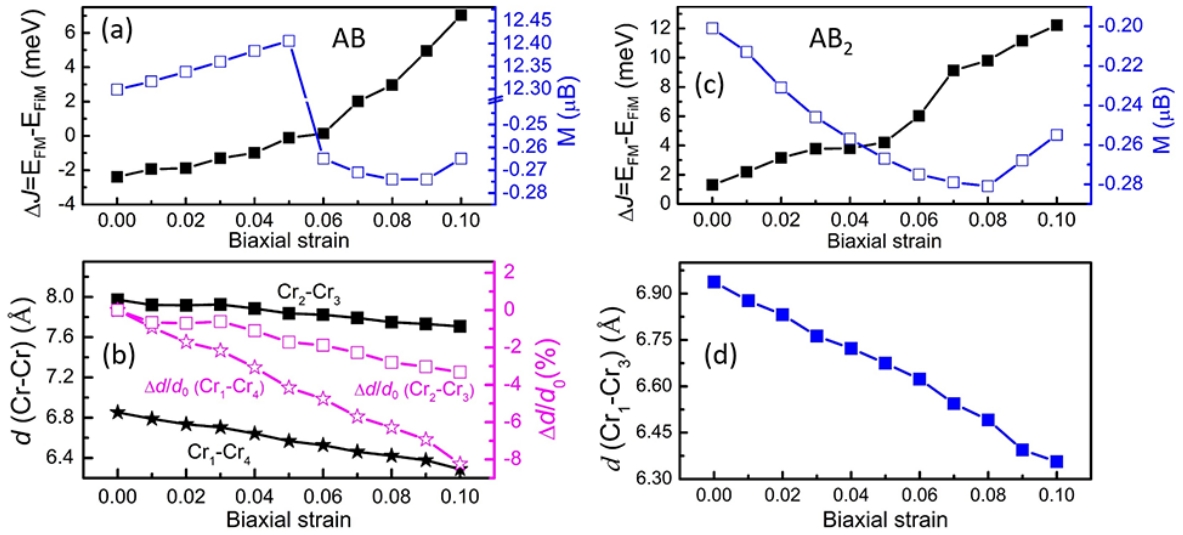

Figure 4. The interlayer exchange energies (ΔJ) and magnetic moments for (a) AB and (c) AB_2 stacking orders under biaxial strains. The variations of Cr-Cr distances from different layer for (b) AB and (d) AB_2 stacking are shown to understanding the changes of interlayer exchange energies. For AB_2 stacking pattern, only NN Cr1-Cr3 interaction because there is no SNN for the case.

We found that the magnetic ground states for various stacking orders of $CrI_3/CrGeTe_3$ heterostructures are influenced strongly by external strains, as shown in Figure 4. Interestingly, a magnetic state transition from FM to FiM is observed for the AB-stacking configuration when strain is larger than a critical value of 6% (Figure 4a), which is reflected by the ΔJ value changing from negative to positive. As a result, the linearly increased total magnetic moment at initial state has a sudden drop from 12.4 μB to -0.27 μB after the critical strain. In contrast, the energy difference ΔJ increases with the increasing strain for AB_2 stacking configuration, implying the FiM stability is enhanced under biaxial strain deformation. The total magnetic moment of the system (magnitude) linearly increases with the strain. The variation of ΔJ value and magnetic moment of AB_1 and AB_2' stacking structures are similar to AB_2 stacking (see Figure S3), while AB_1 stacking preserves the FM magnetic state under strain deformation, which indicates that the biaxial strain can effectively modulated the interlayer magnetic coupling.

The different responses of magnetic states and moments stem from the interlayer magnetic coupling mechanism, namely the competition between NN and SNN exchanges affected by atom distances for $CrI_3/CrGeTe_3$ heterostructures. For AB-stacked configuration, the key to understand this magnetic transition lies in the change of interlayer interaction caused by decreased distance of Cr-Cr between layers. The black lines presented in Figure 4c show that

the Cr1-Cr4 (NN) and Cr2-Cr3 (SNN) distances both decrease linearly with applied tensile strain. While from the pink lines of Figure 4c, the distance of Cr1-Cr4 atoms declines more rapidly compared to that of Cr2-Cr3 according to the ratio changes of $\Delta d/d_0$, resulting in a rise of NN exchange interaction of Cr-Cr between layers. Thus, the AFM coupling caused by Cr1-Cr4 exchange is becoming the dominate factor, and the transition occurred during the increased external stain. For AB_2-stacking, there is only Cr-Cr NN interlayer magnetic exchange as shown in Figure 2, we focused on the distance variation of Cr1-Cr3 under strain. As shown in Figure 4d, the bond lengths of Cr1-Cr3 linearly decrease as a function of the applied tensile strain, leading to an enhanced NN exchange, and thus an enhanced FiM states. The same magnetic mechanism was also discovered and explained in $CrXTe_3$ (X = Si, Ge) systems [34].

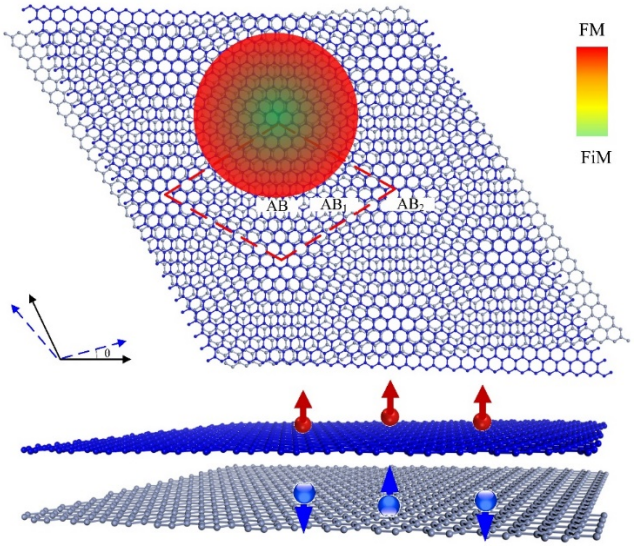

Figure 5: Schematic diagram of the proposed Moiré magnetic domain heterostructures where the magnetic coupling will be controlled by the twisted angle. All the stacking patterns can coexist in the system. For clarity, only the magnetic Cr atoms are shown here while the Cr atoms from different layers are shown in grey and blue balls respectively.

Based on the findings that the magnetic ground state is stacking dependent, we proposed a magnetic domain device in the twisted magnetic heterostructures as in Figure 5. Similar to the recent discovered magic angle in twisted bilayer graphene where the superconductivity can be induced, the Moiré texture will be induced in the heterostructure when CrI_3 is rotated relative to monolayer $CrGeTe_3$, where the all stacking patterns studied above (AB, AB_1, AB_2 and AB_2') can coexist simultaneously. As investigated above, AB and AB_1 stacked areas will be in FM interlayer coupling with large magnetic moments while AB_2 and AB_2' stacked areas will be in FiM states with small magnetic moments. The spin directions from different layers at AB and AB_1 area are the same, while these at AB_2 and AB_2' are opposite, as shown in Figure 5, leading

to the magnetic domains. The size of each stacking area depends on the magnitude of the rotated angle θ, where the periodic lattice length of the Moiré texture can be calculated as $\lambda=a/(2\sin\frac{\theta}{2})$ [38-40]. The interlayer magnetic coupling and domains can be modulated by adjusting the rotation angles and relative position shift between layers. The proposed magnetic device may find extensive application in spintronics and electronics.

4. Conclusions

In summary, using first-principles calculations, we investigated the magnetic states of the heterostructures which combined 2D ferromagnetic semiconductors monolayers CrI_3 and $CrGeTe_3$ with various stacking orders. The magnetic ground states are discovered to depend on the stacking configurations of CrI_3 and $CrGeTe_3$. The underlying mechanism is contribute to the competition between NN and SNN Cr-Cr exchanges in different layers. The FM interlayer coupling is found in AB-, AB_1-stacking while FiM coupling is revealed in AB_2-, AB_2'-stacking configurations, respectively. Besides, the interlayer magnetic coupling, the electronic properties of the heterostructure are also stacking dependent. Taken AB and AB_1 stacking as the examples, it was found that the band gaps are 0.136 and 0.035 eV respectively. More interestingly, the band-edge states are separated into different layers due to the presence of out-of-plane intrinsic polarization. Furthermore, the magnetic coupling of $CrI_3/CrGeTe_3$ heterostructures can be effectively modulated by the biaxial strain, leading to the transition from FM to FiM in AB-stacking after a critical strain due to different variation response of Cr-Cr distance. In other stacking patterns, the intrinsic magnetic coupling will be maintained and enhanced by the strain. Based on the findings of stacking dependent interlayer magnetic coupling, we proposed a magnetic domain device in twisted heterostructures, where all stacking patterns coexist, the magnetic coupling at different location can be controlled by rotation angle and position shift. Our study of 2D magnetic heterostructure unlocks a new approach to tunning the magnetic properties not only for the fundamental researches, but also for the practically switched on/off applications in nano-spintronics.

ASSOCIATED CONTENT

Supporting Information

Differential charge density with Bader charge, band structures and density of states (DOS) for $CrI_3/CrGeTe_3$ heterostructures of AB_1 stacking with FM spin and AB_2' stacking with FiM

configuration. The interlayer exchange energies (ΔJ) and magnetic moments (magnitude) for AB_1 and AB_2' stacking orders under biaxial strains.

Corresponding Author

*E-mail: liangzhi.kou@qut.edu.au

Notes

The authors declare no competing financial interest.

Acknowledgments

We acknowledge the grants of high-performance computer time from computing facility at the Queensland University of Technology, the Pawsey Supercomputing Centre and Australian National Computational Infrastructure (NCI). L.K. gratefully acknowledges financial support by the ARC Discovery Project (DP190101607).

References

1. Gupta, A.; Sakthivel, T.; Seal, S. Recent Development in 2D Materials Beyond Graphene. *Prog. Mater. Sci.* **2015,** *73*, 44-126.

2. Chhowalla, M.; Shin, H. S.; Eda, G.; Li, L. J.; Loh, K. P.; Zhang, H. The Chemistry of Two-dimensional Layered Transition Metal Dichalcogenide Nanosheets. *Nat. Chem.* **2013,** *5* (4), 263-75.

3. Manzeli, S.; Ovchinnikov, D.; Pasquier, D.; Yazyev, O. V.; Kis, A. 2D Transition Metal Dichalcogenides. *Nat. Rev. Mater.* **2017,** *2*, 17033.

4. Li, Y. F.; Zhou Z.; Zhang, S. B. and Chen. Z. F. MoS_2 Nanoribbons: High Stability and Unusual Electronic and Magnetic Properties. *J. Am. Chem. Soc.* **2008,** *130* (49), 16739-16744.

5. Rubén, M. B.; Cristina. G. N.;, Julio. G. H.; Félix. Z. 2D Materials: to Graphene and Beyond. *Nanoscale* **2011,** *3* (1), 20-30.

6. Pesin, D.; MacDonald, A. H. Spintronics and Pseudospintronics in Graphene and Topological Insulators. *Nat. Mater.* **2012,** *11* (5), 409-416.

7. Han, W.; Kawakami, R. K.; Gmitra, M.; Fabian, J. Graphene Spintronics. *Nat. Nanotechnol.* **2014,** *9* (10), 794-807.

8. Han, W. Perspectives for Spintronics in 2D Materials. *APL Materials* **2016,** *4* (3), 032401.

9. Mermin, N. D.; Wagner, H. Absence of Ferromagnetism or Antiferromagnetism in One- or Two-Dimensional Isotropic Heisenberg Models. *Phys. Rev. Lett.* **1966,** *17* (22), 1133-1136.

10. Gong, C.; Li, L.; Li, Z. L.; Ji, H. W.; Stern, A.; Xia, Y.; Cao, T.; Bao, W.; Wang, C. Z.; Wang, Y.; Qiu, Z. Q.; Cava, R. J.; Louie, S. G.; Xia, J.; Zhang, X. Discovery of Intrinsic Ferromagnetism in Two-dimensional Wan der Waals Crystals. *Nature* **2017,** *546* (7657), 265-269.

11. Huang, B.; Clark, G.; Navarro-Moratalla, E.; Klein, D. R.; Cheng, R.; Seyler, K. L.; Zhong, D.; Schmidgall, E.; McGuire, M. A.; Cobden, D. H.; Yao, W.; Xiao, D.; Jarillo-Herrero, P.; Xu, X. D. Layer-dependent Ferromagnetism in a Van der Waals Crystal down to the Monolayer Limit. *Nature* **2017,** *546* (7657), 270-273.

12. Zhang, W. B.; Qu, Q.; Zhu, P.; Lam, C. H. Robust Intrinsic Ferromagnetism and Half Semiconductivity in Stable Two-dimensional Single-layer Chromium Trihalides. *J. Mater. Chem. C,* **2015,** *3* (48), 12457-12468.

13. Soriano, D.; Cardoso, C.; Fernández-Rossier, J., Interplay between interlayer exchange and stacking in CrI_3 bilayers. *Solid State Commun.* **2019,** *299*, 113662.

14. Jiang, S.; Shan, J.; Mak, K. F., Electric-field switching of two-dimensional van der Waals magnets. *Nat Mater* **2018,** *17* (5), 406-410.

15. Jiang, P. H.; Wang, C.; Chen, D. C.; Zhong, Z. C.; Yuan, Z.; Lu, Z. Y.; Ji, W. Stacking Tunable Interlayer Magnetism in Bilayer CrI_3. *Phys. Rev. B* **2019,** *99* 144401.

16. Huang, B.; Clark, G.; Klein, D. R.; MacNeill, D.; Navarro-Moratalla, E.; Seyler, K. L.; Wilson, N.; McGuire, M. A.; Cobden, D. H.; Xiao, D.; Yao, W.; Jarillo-Herrero, P.; Xu, X. D. Electrical Control of 2D Magnetism in Bilayer CrI_3. *Nat. Nanotechnol.* **2018,** *13* (7), 544-548.

17. Morell, E. S.; León, A.; Miwa, R. H.; Vargas, P. Control of Magnetism in Bilayer CrI_3 by an External Electric Field. *2D Materials* **2019,** *6*, 025020.

18. Webster, L.; Yan, J. A. Strain-tunable Magnetic Anisotropy in Monolayer $CrCl_3$,$CrBr_3$,and CrI_3. *Phys. Rev. B* **2018,** *98* 144411.

19. Trambly de Laissardiere, G.; Mayou, D.; Magaud, L. Localization of Dirac Electrons in Rotated Graphene Bilayers. *Nano Lett.* **2010,** *10* (3), 804-808.

20. Yankowitz, M.; Xue, J. M.; Cormode, D.; Sanchez-Yamagishi, J. D.; Watanabe, K.; Taniguchi, T.; Jarillo-Herrero, P.; Jacquod, P.; LeRoy, B. J. Emergence of Superlattice Dirac Points in Graphene on Hexagonal Boron Nitride. *Nat. Phys.* **2012,** *8* (5), 382-386.

21. Avsar, A.; Tan, J. Y.; Taychatanapat, T.; Balakrishnan, J.; Koon, G. K. W.; Yeo, Y.; Lahiri, J.; Carvalho, A.; Rodin, A. S.; O'Farrell, E. C. T.; Eda, G.; Castro Neto, A. H.; Özyilmaz, B. Spin-orbit Proximity Effect in Graphene. *Nat. Commun.* **2014,** *5*, 4875.

22. Fang, H.; Battaglia, C.; Carraro, C.; Nemsak, S.; Ozdol, B.; Kang, J. S.; Bechtel, H. A.; Desai, S. B.; Kronast, F.; Unal, A. A.; Conti, G.; Conlon, C.; Palsson, G. K.; Marting, M. C.; Minor, A. M.;

Fadley, C. S.; Yablonovitch, E.; Maboudian, R.; and Javey. A. Strong Interlayer Coupling in Van der Waals Heterostructures Built from Single-layer Chalcogenides. *PNAS* **2014,** *111*, 6198–6202.

23. Jiang, S. W.; Li, L. Z.; Wang, Z. F.; Mak, K. F.; Shan, J. Controlling Magnetism in 2D CrI_3 by Electrostatic Doping. *Nat. Nanotechnol.* **2018,** *13* (7), 549-553.

24. Seyler, K. L.; Zhong, D.; Huang, B.; Linpeng, X. Y.; Wilson, N. P.; Taniguchi, T.; Watanabe, K.; Yao, W.; Xiao, D.; McGuire, M. A.; Fu, K. C.; Xu, X. D. Valley Manipulation by Optically Tuning the Magnetic Proximity Effect in WSe_2/CrI_3 Heterostructures. *Nano Lett.* **2018,** *18* (6), 3823-3828.

25. Kresse, G.; Furthmüller. J. Efficiency of Ab-initio Total Energy Calculations for Metals and Semiconductors Using a Plane-wave Basis Set. *Comput. Mater. Sci* **1996,** *6* (1), 15.

26. Kresse, G.; Joubert. D. From Ultrasoft Pseudopotentials to The Projector Augmented-wave Method. *Phys. Rev. B* **1999,** *59*, 1758.

27. Perdew, J. P.; Kurke. B., Ernzerhof. M. Generalized Gradient Approximation Made Simple. *Phys. Rev. Lett.* **1996,** *77*, 3865.

28. Grimme, S.; Antony, J.; Ehrlich, S.; Krieg, H. A Consistent and Accurate Ab Initio Parametrization of Density Functional Dispersion Correction (DFT-D) for the 94 Elements H-Pu. *J. Chem. Phys.* **2010,** *132* (15), 154104.

29. Monkhorst, H. J.; Pack, J. D. Special Points for Brillouin-zone Integrations. *Phys. Rev. B* **1976,** *13* (12), 5188-5192.

30. Wang, H.; Fan, F. R.; Zhu, S. S.; Wu, H. Doping Enhanced Ferromagnetism and Induced Half-metallicity in CrI_3 Monolayer. *EPL (Europhysics Letters)* **2016,** *114* (4), 47001.

31. Sivadas, N.; Daniels, M. W.; Swendsen, R. H.; Okamoto, S.; Xiao, D. Magnetic Ground State of Semiconducting Transition-metal Trichalcogenide Monolayers. *Phys. Rev. B* **2015,** *91* 235425.

32. McGuire, M. A.; Dixit, H.; Cooper, V. R.; Sales, B. C. Coupling of Crystal Structure and Magnetism in the Layered, Ferromagnetic Insulator CrI_3. *Chem. Mater.* **2015,** *27* (2), 612-620.

33. Huang, C. X.; Feng, J. S; Wu, F.; Ahmed, D.; Huang, B.; Xiang, H. J.; Deng, K. M.; Kan, E. J. Toward Intrinsic Room-Temperature Ferromagnetism in Two-Dimensional Semiconductors. *J. Am. Chem. Soc.* **2018,** *140* (36), 11519-11525.

34. Li, X. X., Yang. J. L. $CrXTe_3$ (X = Si, Ge) Nanosheets: Two Dimensional Intrinsic Ferromagnetic Semiconductors. *J. Mater. Chem. C* **2014,** *2* (34), 7071-7076.

35. Sivadas, N.; Okamoto, S.; Xu, X. D.; Fennie, C. J.; Xiao, D. Stacking-Dependent Magnetism in Bilayer CrI_3. *Nano Lett.* **2018,** *18* (12), 7658-7664.

36. Song, T.; Fei, Z.; Yankowitz, M.; Lin, Z.; Jiang, Q.; Hwangbo, K.; Zhang, Q.; Sun, B.; Taniguchi, T.; Watanabe, K.; McGuire, M. A.; Graf, D.; Cao, T.; Chu, J. H.; Cobden, D. H.; Dean, C. R.; Xiao, D.; Xu, X., Switching 2D magnetic states via pressure tuning of layer stacking. *Nat Mater* **2019,** *18* (12), 1298-1302.

37. Li, T.; Jiang, S.; Sivadas, N.; Wang, Z.; Xu, Y.; Weber, D.; Goldberger, J. E.; Watanabe, K.; Taniguchi, T.; Fennie, C. J.; Fai Mak, K.; Shan, J., Pressure-controlled interlayer magnetism in atomically thin CrI_3. *Nat Mater* **2019,** *18* (12), 1303-1308.

38. Kobayashi, K., Moiré pattern in scanning tunneling microscopy: Mechanism in observation of subsurface nanostructures. *Phys. Rev. B* **1996,** *53*, 11091.

39. Warner, J. H.; Rümmelim, M. H.; Gemming, T.; Büchner, B.; and Briggs, G. A. D. Direct Imaging of Rotational Stacking Faults in Few Layer Graphene. *Nano Lett.* **2009,** *9* (1), 102-106.

40. Tong, Q. J.; Liu, F.; Xiao J.; and Yao W. Skyrmions in the Moiré of van der Waals 2D Magnets. *Nano Lett.* **2018,** *18*, 7194-7199.